NJC

PAPER

View Article Online
View Journal | View Issue

Cite this: *New J. Chem.*, 2015, 39, 6108

New insight into high-temperature driven morphology reliant $CoMoO_4$ flexible supercapacitors†

John Candler,[a] Tyler Elmore,[a] Bipin Kumar Gupta,[b] Lifeng Dong,[c] Soubantika Palchoudhury[d] and Ram K. Gupta*[a]

Received (in Montpellier, France) 21st February 2015,
Accepted 26th May 2015

DOI: 10.1039/c5nj00446b

www.rsc.org/njc

A facile hydrothermal method has been successfully developed for the synthesis of cobalt molybdate ($CoMoO_4$). The morphology of the $CoMoO_4$ was tailored by varying the growth conditions, and as a result different morphologies have been achieved such as cauliflower, brick and nano-sphere structures. The proposed potential use of the $CoMoO_4$ as an electrode material for flexible supercapacitor applications was examined using cyclic voltammetry (CV) and galvanostatic charge–discharge measurements. It was observed that the specific capacitance of $CoMoO_4$ depends on its morphology. A specific capacitance of 169 F g^{-1} in 3 M KOH at a current of 1 mA was observed for the nano-sphered $CoMoO_4$. The effect of the electrolyte (LiOH, NaOH and KOH) on the electrochemical properties of the $CoMoO_4$ was also investigated. The specific capacitance depends on the type of electrolyte and showed the highest value of 259 F g^{-1} in a 3 M NaOH electrolyte. Furthermore, these electrodes showed excellent cyclic stability. We have fabricated a flexible supercapacitor device by sandwiching two electrodes separated by an ion-transporting layer. The device shows no degradation in its capacitive properties upon bending and shows improved stability with the number of cyclic CV performances. The effect of temperature on the charge storage properties of the device was also investigated for high temperature applications. The specific capacitance of the device significantly increased when the operational temperature of the device was elevated from 10 to 70 °C. Hence, this study provides an ultimate facile method to synthesize morphology controlled cobalt molybdate for applications in the next generation of flexible energy storage devices, which can perform more efficiently at a higher temperature.

1. Introduction

Supercapacitors are considered the most prominent and efficient energy storage devices next to lithium ion batteries due to their high power densities, fast charge–discharge capabilities and long cyclibility.[1–6] Supercapacitors possess high power density as compared to batteries and they are able to solve the increasing demand for energy in small consumer products, electrical vehicles and devices wherein quick power delivery is highly desired.[7–10] Supercapacitors are classified into two categories based on their charge storage mechanism. The first group of capacitors is called as electrical double-layer capacitors (EDLCs), wherein the charge is stored at the interface. The second group is recognized as redox electrochemical capacitors (pseudocapacitors), wherein the charge storage arises due to Faradaic reactions at the electrode/electrolyte interface.[1,11] Although the pseudocapacitors have a higher charge storage capacity compared to EDLCs, they suffer from high cost and poor cyclic stability. The charge-storage capacity of pseudocapacitors largely depends on the redox process at the electrode/electrolyte interface, and their performance can be improved using nano-structured redox active materials.[12–14]

Several redox active metal oxides and sulfides, such as iron oxide, nickel oxide, ruthenium oxide, cobalt oxide, manganese oxide, molybdenum sulfide and cobalt sulfide, have been used for supercapacitor applications.[14–28] Recently, metal molybdates have attracted considerable research interest for supercapacitor applications due to their excellent electrochemical performance, low cost and environmental friendliness.[29] Mai *et al.*[30] synthesized three-dimensional $MnMoO_4/CoMoO_4$ hetero-structures.

[a] *Department of Chemistry, Pittsburg State University, 1701 S. Broadway, Pittsburg, KS 66762, USA. E-mail: ramguptamsu@gmail.com; Fax: +1 620 2354003; Tel: +1 620 2354763*
[b] *National Physical Laboratory (CSIR), Dr K.S. Krishnan Road, New Delhi 110012, India*
[c] *Physics, Astronomy, and Materials Science, Missouri State University, 901 S. National Avenue, Springfield, MO 65897, USA*
[d] *Center for Materials for Information Technology, The University of Alabama, Tuscaloosa, AL-35487, USA*

† Electronic supplementary information (ESI) available. See DOI: 10.1039/c5nj00446b

These hetero-structures showed a specific capacitance of 187.1 F g^{-1} at a current density of 1 A g^{-1} with good reversibility and cyclic efficiency. The electrochemical properties of nanorods and hierarchical nanospheres of $NiMoO_4$ have been well studied and compared with respect to their morphology.[31] The nanospheres of $NiMoO_4$ showed a higher specific capacitance and better cycling stability due to their large surface area and high electrical conductivity.

Xia *et al.*[32] used a facile hydrothermal method to synthesize $CoMoO_4$–graphene for supercapacitor applications. The $CoMoO_4$–graphene composite showed a specific capacitance of about 394.5 F g^{-1} from the CV curve at 1 mV s^{-1}, which was higher than that found for pure-$CoMoO_4$ (72.0 F g^{-1}). A facile sonochemical method was also used for the synthesis of $CoMoO_4$ nanostructures for supercapacitor applications.[33] The CV curves showed the presence of redox pairs, which confirms the pseudocapacitive nature of $CoMoO_4$. The galvanostatic charge–discharge studies showed a maximum specific capacitance of 133 F g^{-1} at a constant discharge current density of 1 mA cm^{-2}. A microwave assisted synthesis of reduced graphene oxide–cobalt molybdate (RGO–$CoMoO_4$) nano-composites was reported.[34] The resulting nanocomposites showed well-anchored $CoMoO_4$ nanoparticles on the graphene sheets. The specific capacitance of $CoMoO_4$ improved from 95.0 F g^{-1} to about 322.5 F g^{-1} by fabricating the nanocomposite with reduced graphene oxide.

Recently, Liu *et al.*[35] studied the effect of calcination temperature on the electrochemical properties of $CoMoO_4$. It was observed that the high crystallinity induced by calcination at high temperature is unfavorable to improve the supercapacitive performance of $CoMoO_4$. In the present study, we report a detailed investigation on the effect of the morphology on the charge storage capacity of $CoMoO_4$. $CoMoO_4$ was grown under different conditions to tailor the morphology using a facile hydrothermal method. The results obtained from the electrochemical study suggest that the charge storage capacity largely depends on the morphology of the $CoMoO_4$. A highest specific capacitance of 259 F g^{-1} with excellent cyclic and flexibility stability was observed. The effect of temperature on the capacitive properties of the supercapacitor device was tested from 10 to 70 °C. It was observed that the device works better at higher temperature. The electrochemical results strongly suggest the potential application of cobalt molybdate as a flexible electrode material for high performance and stable supercapacitor, which is a requirement for today's needs.

2. Experimental details

$Na_2MoO_4{\cdot}2H_2O$ and $Co(CH_3COO)_2{\cdot}4H_2O$ of analytical grade were used in the experiments without further purification. Other chemicals, such as ethanol and ethylene glycol, were also of analytical grade. In a typical synthesis, 1 mmol of $Na_2MoO_4{\cdot}2H_2O$ and 1 mmol of $Co(CH_3COO)_2{\cdot}4H_2O$ were dissolved in 30 mL of water (CMO-1), 30 mL of a (1 : 1 v/v) ethanol–water mixture (CMO-2) and 30 m of ethylene glycol (CMO-3) using ultrasonication. Then, the obtained solution was placed into a 50 mL autoclave with a Teflon liner. The autoclave was maintained at 150 °C for 12 hours. Subsequently, the autoclave was cooled naturally in air. The resulting black precipitates were filtered, washed several times with distilled water and dried at 500 °C for 4 hours.

Structural characterization of the cobalt molybdate powder samples was performed using X-ray diffraction (XRD) and scanning electron microscopy (SEM). The XRD patterns were recorded with a Shimadzu X-ray diffractometer using the 2θ–θ scan with $CuK\alpha_1$ (λ = 1.5406 Å) radiation, which was operated at 40 kV and 30 mA. The particle size and morphology of cobalt molybdates were studied using a JEOL JSM-840A scanning electron microscope and an FEI Quanta 200 field emission scanning electron microscope (FESEM) equipped with an Oxford INCA 250 silicon drift X-ray energy dispersive spectrometer (EDS).

The electrochemical measurements were performed using a standard three electrode system on a Versastat4-500 electrochemical workstation (Princeton Applied Research, USA). The working electrode was prepared by mixing 80 wt% of the synthesized cobalt molybdate powder, 10 wt% of acetylene black and 10 wt% of polyvinylidene difluoride (PVdF) in the presence of *N*-methyl pyrrolidinone (NMP). After mixing the components, the slurry was pasted onto nickel foam. The prepared electrode was dried at 60 °C under vacuum for 10 h. The loading mass of CMO-1, CMO-2 and CMO-3 was 1.78, 1.22 and 2.28 mg, respectively. The loading mass of cobalt molybdate was accurately measured by weighing the nickel foam before and after electrode preparation using an analytical balance (model MS105DU, Mettler Toledo, max. 120 g, 0.01 mg of resolution). A platinum wire and a saturated calomel electrode (SCE) were used as a counter electrode and reference electrode, respectively. 3 M KOH, NaOH and LiOH were used as the electrolyte. The performance of the supercapacitors was evaluated by cyclic voltammetry (CV) and galvanostatic charge–discharge techniques. The flexible device was assembled using two working electrodes separated by an ion-transporting layer (Celgard, 25 μm thick, 39% porosity) in a NaOH electrolyte. Before assembling the device, both working electrodes and ion transporting layer were soaked in the electrolyte for 1 h.

3. Results and discussion

The morphology controlled synthesis of cobalt molybdate was performed using an ultrasonic assisted hydrothermal method. The chemical reaction for the formation of cobalt molybdate is given below:

$$Co(CH_3COO)_2{\cdot}4H_2O + Na_2MoO_4 \cdot 2H_2O \xrightarrow[\text{HYDROTHERMAL}]{\text{ULTRASONIC}} CoMoO_4 \cdot H_2O \quad (1)$$

$$CoMoO_4 \cdot H_2O \xrightarrow{500\,^{\circ}C-4h} CoMoO_4 \quad (2)$$

The synthesized cobalt molybdate and the fabricated electrodes were structurally and electrochemically characterized for their potential applications as a flexible electrode for supercapacitors. In the following sections, we present the details of our observations and discussions.

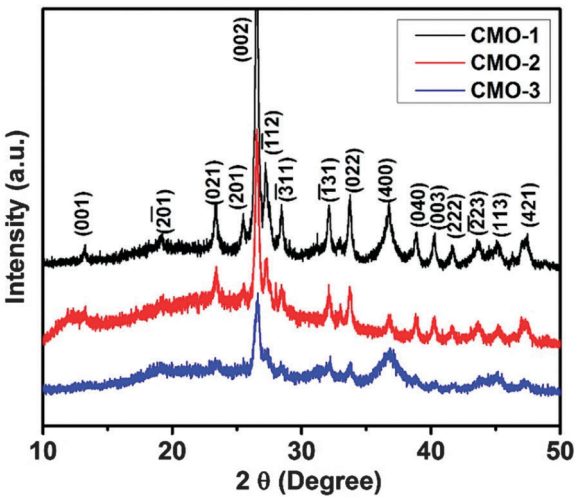

Fig. 1 XRD patterns of the cobalt molybdate synthesized with different morphologies.

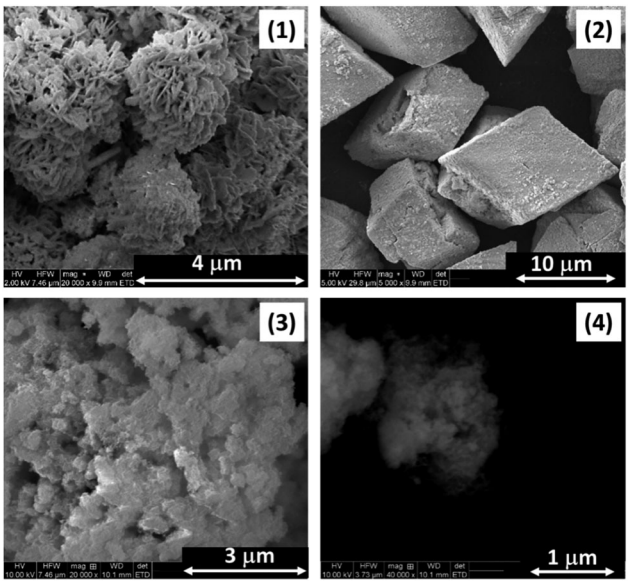

Fig. 2 SEM images of (1) CMO-1, (2) CMO-2, and (3) CMO-3. (4) magnified view of CMO-3.

The crystal structure and phase purity of cobalt molybdates were studied using XRD measurements. The X-ray diffraction patterns of the synthesized cobalt molybdates are shown in Fig. 1. The diffraction peaks at 13.22, 19.18, 23.34, 25.46, 26.51, 27.26, 28.48, 32.14, 32.87, 33.76, 36.74, 38.78, 40.27, 41.65, 43.75, 45.14, and 47.44 can be assigned to the reflections of the (001), (201), (021), (201), (002), (112), (311), (131), (022), (222), (400), (040), (003), (222), (223), (113), and (421) planes, respectively. The XRD patterns are in good agreement with the standard pattern of $CoMoO_4$ (JCPDF, card no. 21-0868). The absence of any other impurity peaks except $CoMoO_4$ peaks suggests that the synthesized materials are phase pure.

Furthermore, the effects of the growth conditions on the morphology and size of cobalt molybdate were studied in details using scanning electron microscopy. SEM images of cobalt molybdate grown under different conditions are shown in Fig. 2. As can be seen in the SEM images, the structure and morphology of the CMO largely depends on the growth conditions. The cobalt molybdate synthesized in water shows cauliflower-like morphology (CMO-1), whereas just by changing the water to an ethanol–water (1 : 1 v/v) mixture, the morphology becomes solid brick-like (CMO-2). Interestingly, using ethylene glycol as the solvent, the morphology of cobalt molybdate changes to a nanostructure (CMO-3) with high porosity. The nanostructure of the synthesized cobalt molybdate in ethylene glycol is also revealed in the XRD analysis. The broad peaks observed in the XRD patterns of CMO-3 suggest its nanostructure. The nanostructured materials show higher full width half maximum in the XRD patterns as compared to the microstructured materials. TEM measurements were conducted to further investigate the microstructural properties of cobalt molybdates. Fig. 3 shows the TEM images of CMO-1, CMO-2 and CMO-3. The TEM results reveal that cobalt molybdates are associated with a porous morphology. Energy dispersive X-ray spectroscopy (EDS) of CMO-3 shows the presence of Co, Mo, O, C, and Cu (Fig. S1, ESI†). The presence of Cu is due to the conductive copper tape used in the EDS measurement. The relative concentration ratio of Co, Mo and O was observed to be about 1 : 1 : 4, which further confirms the $CoMoO_4$ phase.

Furthermore, the effect of morphology on the charge storage capacity of cobalt molybdate was investigated using electrochemical studies. Electrochemical measurements were performed using cyclic voltammetry and galvanostatic charge discharge measurements. Fig. 4a shows the cyclic voltammetry (CV) curves for cobalt molybdates at a scan rate of 50 mV s^{-1} in a 3 M KOH electrolyte. All the cobalt molybdate samples show a pair of redox (anodic and cathodic) peaks. The area under the CV curves was observed to be the highest for CMO-3. Based on the initial observations, detailed electrochemical studies on CMO-3 sample were performed. Fig. 4b shows the CV curves for CMO-3 at various scan rates. It was found that the area under the CV curves increases with increase in scan rates. It was further observed that the peak current increases with an increase in the scan rate and the difference in the cathodic and anodic peak potential expands gradually.

A linear relationship was observed for the peak current and the square root of the scan rate (Fig. S2, ESI†). The linear behavior between the peak current and the square root of the scan rate indicates that the reaction kinetics during the redox process are likely controlled by diffusion processes. The potential application of cobalt molybdate for flexible charge storage devices was tested using CV at various bending angles. Fig. 5 shows the CV curves of CMO-3 at various bending angles. The CV curves at various bending angles show identical shape, indicating the high electrochemical stability of cobalt molybdate electrode upon bending. The results suggest that cobalt molybdate could have high potential as an electrode material for flexible charge storage devices.

The effects of an applied current on the charge storage capacity of cobalt molybdates were studied using galvanostatic

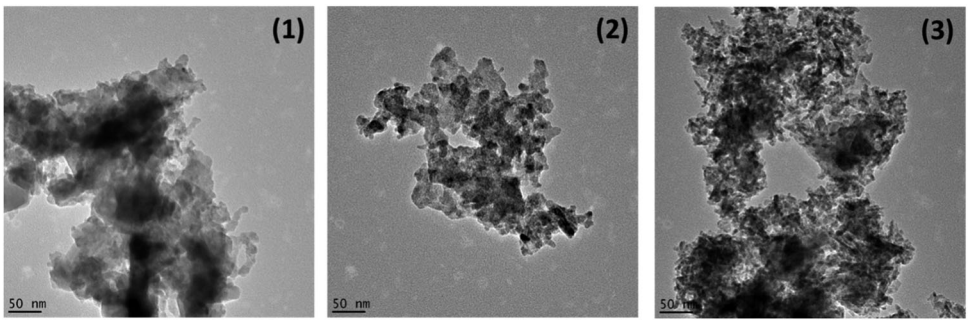

Fig. 3 TEM images of (1) CMO-1, (2) CMO-2 and (3) CMO-3.

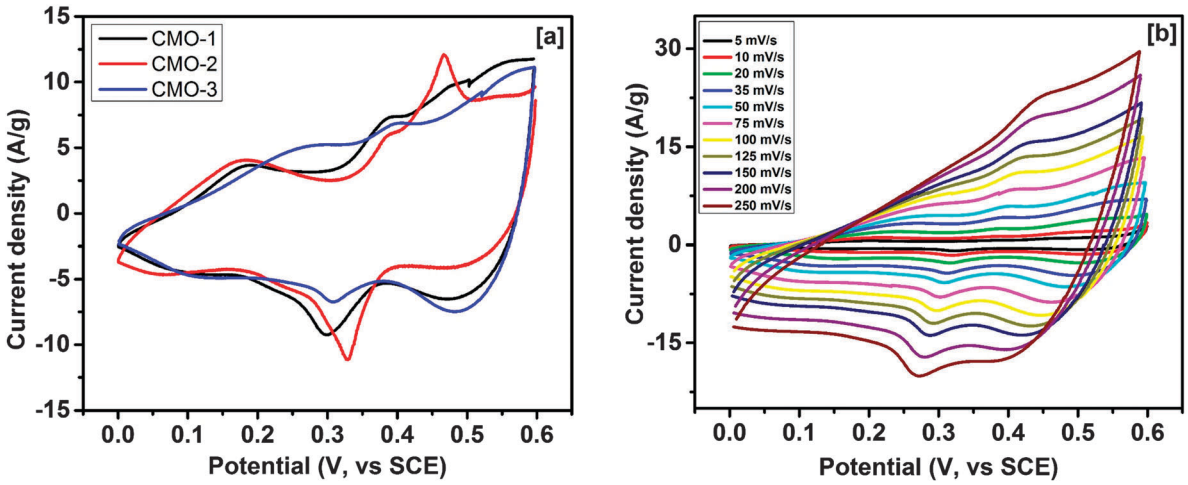

Fig. 4 CV curves for (a) all the samples at 50 mV s^{-1} in a 3 M KOH electrolyte and (b) CMO-3 at various scan rates in a 3 M KOH electrolyte.

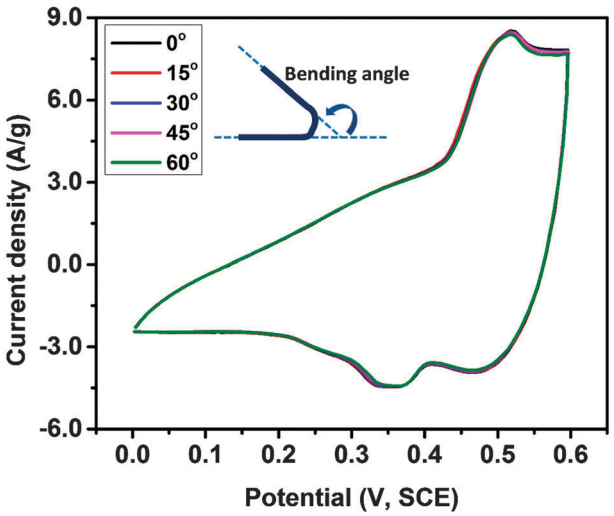

Fig. 5 CV curves for CMO-3 at various bending angles.

charge–discharge characteristics. The galvanostatic charge–discharge characteristics of cobalt molybdates in a 3 M KOH electrolyte are shown in Fig. S3 (ESI†). Fig. 6 shows the charge–discharge characteristics of CMO-3 at various applied currents in 3 M KOH and LiOH electrolytes. As seen in the Fig. 6, the charge–discharge curves are highly symmetric in shape, indicating high electrochemical reversibility and fast reaction kinetics.[36,37] In addition to the symmetrical charge–discharge profile, it was observed that the charge–discharge time depends on the electrolyte. The charge–discharge time (and thus the capacitance) was observed to be at a maximum in the LiOH electrolyte. This could be due to the smaller ionic size of the Li ions. The smaller ions could approach the surface of the cobalt molybdate easily and more effectively.

The specific capacitance (C_{sp}) of the cobalt molybdate electrode was calculated using the equation below:

$$C_{sp} = \frac{I \times \Delta t}{\Delta V \times m} \quad (3)$$

where I is the discharge current (A), Δt is the discharge time (s), ΔV is the potential window (V) and m is the mass (g) of the active material. Fig. 7a shows the variation of the specific capacitance *versus* discharge currents for all the samples in a 3 M KOH electrolyte. The specific capacitance of the samples decreases with an increasing current. The decrease in the specific capacitance with the increase of the discharge current could be due to an increase in the potential drop and insufficient faradic redox reactions at higher discharge currents. A specific capacitance of 158, 142 and 169 F g^{-1} were observed for CMO-1,

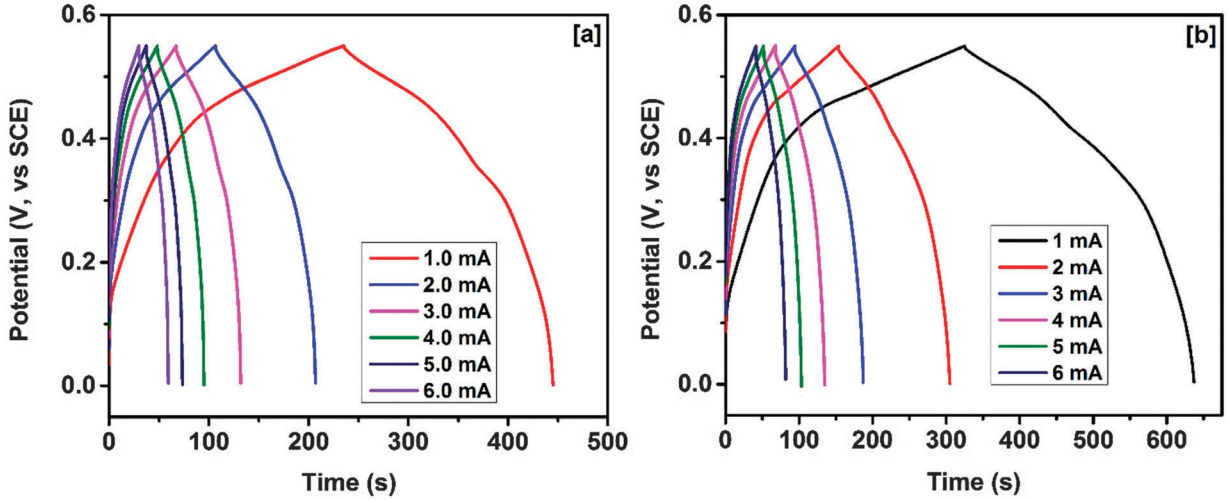

Fig. 6 Galvanostatic charge–discharge characteristics for CMO-3 at different currents in a (a) 3 M KOH and (b) 3 M LiOH electrolyte.

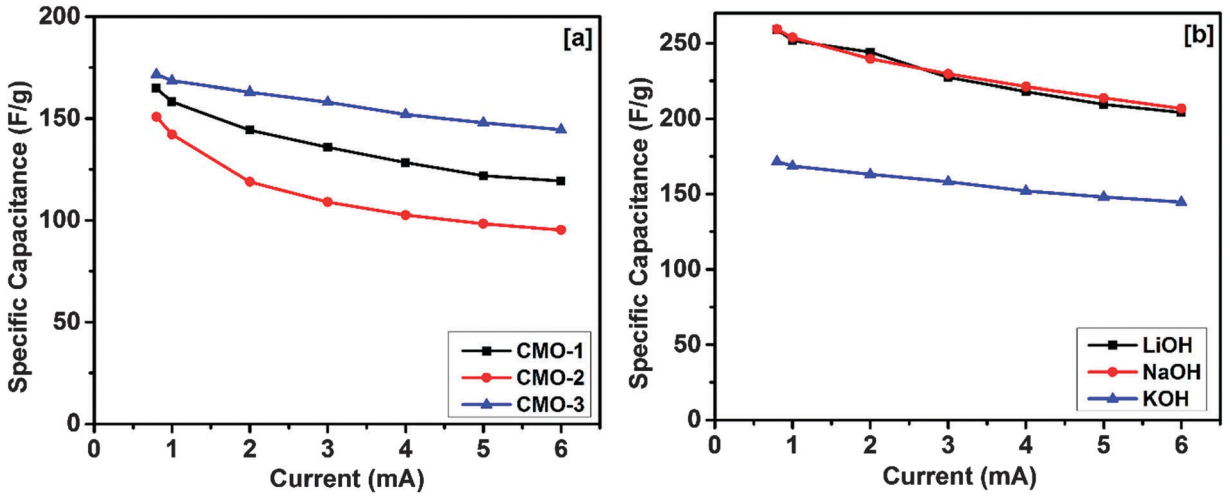

Fig. 7 Variation of the specific current *versus* current for (a) all the samples in a 3 M KOH electrolyte, and (b) CMO-3 in 3 M LiOH, NaOH and KOH electrolytes.

CMO-2 and CMO-3, respectively, at 1 mA of discharge current. Veerasubramani *et al.*[33] used a sonochemical method to synthesis $CoMoO_4$. They observed a specific capacitance of $\sim$133 F g^{-1} in a KOH electrolyte. The higher specific capacitance observed for our hydrothermally synthesized CMO-3 could be due to its nanostructure. The nanostructured materials offer a higher surface area for redox reactions, which results in a higher specific capacitance. The effect of the ionic size in the electrolyte was also investigated. Fig. 7b shows the variation of the specific capacitance for CMO-3 with the discharge current in different electrolytes. As seen, Li^+ and Na^+ have an almost similar effect on the charge storage capacity. On the other hand, a KOH electrolyte shows the minimum charge storage when compared to LiOH and NaOH, which could be due to the larger ionic radius of K^+.

The performance of the supercapacitors was further evaluated using a Ragone plot, which relates the energy density to the power density of a material. The energy density and the power density for a supercapacitor cell can be calculated using the following equations:[38]

$$E(\text{W h kg}^{-1}) = \frac{C_{sp} \times \Delta V^2}{7.2} \quad (4)$$

$$P(\text{W kg}^{-1}) = \frac{E \times 3600}{t} \quad (5)$$

where C_{sp} (F g^{-1}) is the specific capacitance calculated from charge–discharge characteristics, ΔV (V) is the potential window and t (s) is the discharge time. In Fig. 8a and b, we show the plots for the specific energy density and power density of all the samples measured in a 3 M KOH electrolyte and CMO-3 in all three electrolytes, respectively. CMO-2 delivers the maximum power density but its energy density is low. On the other hand, CMO-3 delivers both very high power density and energy density in the LiOH and NaOH electrolytes (Fig. 8b). Veerasubramani *et al.*[33] reported the values for the energy density and power

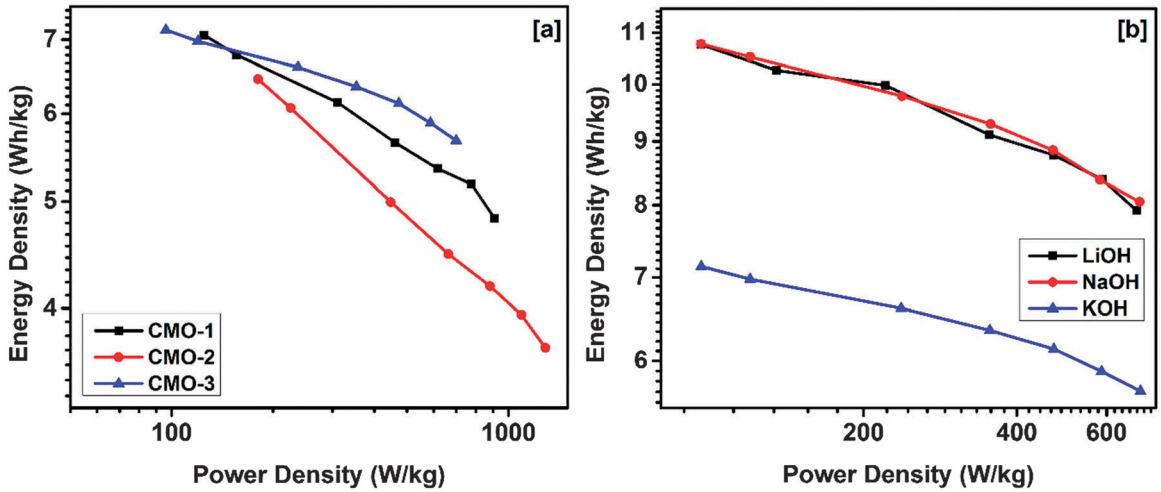

Fig. 8 Variation of the power density *versus* energy density for (a) all the samples in a 3 M KOH electrolyte and (b) CMO-3 in 3 M LiOH, NaOH and KOH electrolytes.

density as 9.06 W h kg^{-1} and 69.9 W kg^{-1}, respectively at a discharge current density of 1 mA cm^{-2} for sonochemically synthesized cobalt molybdate.

Fig. 9 shows the variation of the specific capacitance with the charge–discharge cycles for CMO-3 in a 3 M NaOH electrolyte. The inset of Fig. 9 shows first few cycles of the charge–discharge curves for the same sample. As seen, the specific capacitance of the electrode slowly increases with the number of charge–discharge cycles. The increase in the capacitance with the cyclic charge–discharge process could be due to activation of the cobalt molybdate surface with time. This makes the surface of cobalt molybdate in full contact with the electrolyte, which leads to the improved electrochemical performance.[35,39] The results obtained from the electrochemical studies show that cobalt molybdate could be used as a high performance material for flexible charge storage devices.

The electrochemical properties of the supercapacitor device (Fig. S4, ESI†) were studied to investigate its applicability as a flexible device, which could operate at elevated temperature. The as fabricated device was lightweight and highly flexible. The CV curves for the device as a function of bending angle are shown in Fig. 10. The device was bended manually at various angles for electrochemical testing. The CV curves demonstrate that there is no significant change (less than 0.5%) in the charge storage capacity of the device upon bending, which suggests that the device can be successfully used as a flexible charge storage device. The effect of scan rate on the CV curves of the device was studied (Fig. S5, ESI†). The rectangular shapes and symmetry of the CV curves indicate near an ideal pseudocapacitive nature of the device, even at the high scan rates. The inset of Fig. S5 (ESI†) shows the specific capacitance of the device as a function of scan rates. The specific

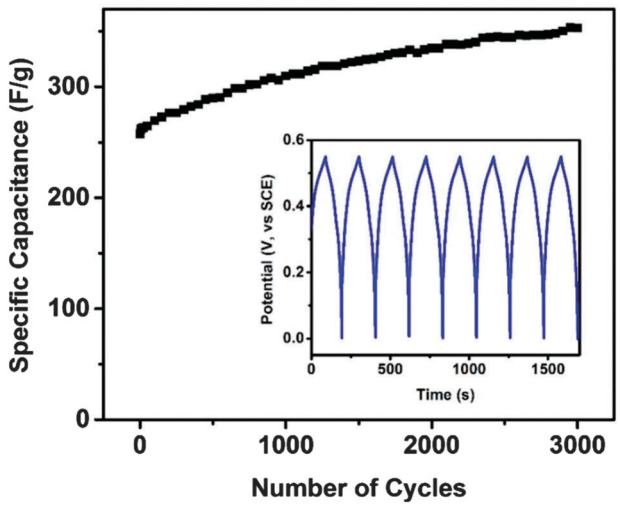

Fig. 9 Variation of the specific capacitance *versus* the number of discharge cycles. The inset figure shows the first few charge–discharge cycles.

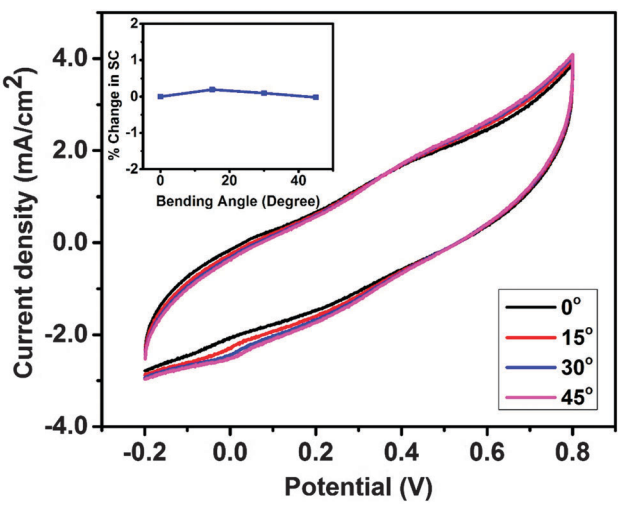

Fig. 10 CV curves for the supercapacitor device at various bending angles. The inset figure shows the change in the specific capacitance (SC) as a function of bending angle.

capacitance (C_{sp}) of the device was calculated using the following expression:[40]

$$C_{sp} = \frac{Q}{\Delta V \times \left(\frac{\partial v}{\partial t}\right) \times A} \quad (6)$$

where Q is the area under the CV curve, $\partial v/\partial t$ is the scan rate, ΔV is the potential window and A is the area of the device. The specific capacitance of the device decreases from 0.57 to 0.08 F cm^{-2} with an increasing scan rate from 10 mV s^{-1} to 200 mV s^{-1}, respectively. The decrease in the specific capacitance with an increase in the scan rate could be due to an insufficient time for the electrochemical reactions to occur. At a higher scan rate, the concentration of the ions at the electrode/electrolyte interface is high and the diffusion rate for the electrolyte from the electrode/electrolyte interface to electrode may be not enough to satisfy the electrochemical reactions.[41]

The long-term cyclic stability of the device was studied using cyclic voltammetry. Fig. 11 shows the CV curves for the device at various cycles. The shape and area of the voltammograms were nearly identical, suggesting the high cyclic stability of the fabricated device. The inset of Fig. 11 shows the percentage retention of the specific capacitance as a function of the number of cycles. It was observed that the specific capacitance of the device first decreases and then increases up to 3000 cycles. The improved cyclic stability of the device could be due to a gradual access of electrolyte ions to the active sites of the electrodes surface with the continuous cycles. Yuan *et al.*[42] have also observed a similar improvement in the specific capacitance upon cycling for a hierarchically porous Co_3O_4 film. Ouassim Ghodbane *et al.*[43] also reported the improvement in the capacitive properties of an electrochemical supercapacitor based on MnO_2.

The electrochemical properties are dependent on temperature. Therefore, we studied the effect of temperature on the charge storage capacity of the device for their applications in harsh temperature environments. Fig. 12 shows the CV curves for the device at various temperatures. The shapes of the voltammograms are very similar even at higher temperatures, indicating a near ideal capacitive behavior within this wide temperature window. It was further observed that the specific capacitance of the device increases with increasing temperature. The inset of Fig. 12 shows the percentage increase in the capacitance of the device with temperature. The device showed an increase of 386% in the specific capacitance when the working temperature was increased from 10 to 70 °C. The SEM images of the electrode material before and after electrochemical testing were very similar, indicating no structural damage of the cobalt molybdate (Fig. S6, ESI†). This indicates that cobalt molybdates are more suitable for charge storage applications at elevated higher temperature rather than low temperature conditions.

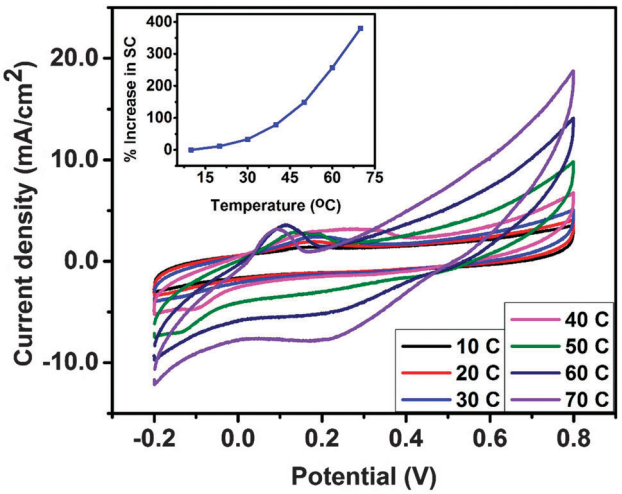

Fig. 12 CV curves for the supercapacitor device at various temperatures. Inset figure shows the % increase in the specific capacitance of the device with temperature.

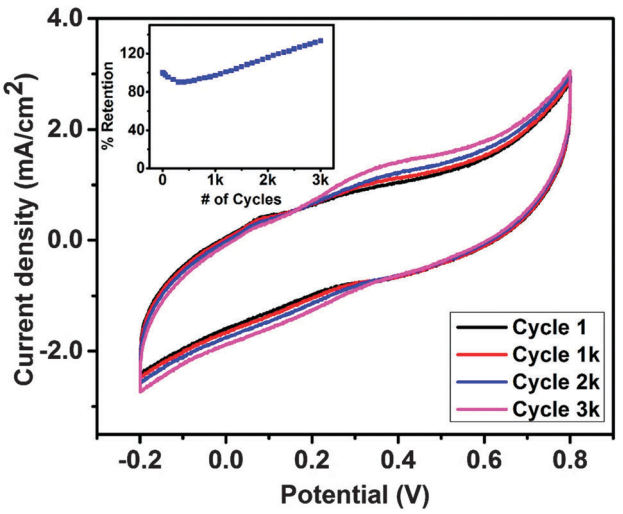

Fig. 11 CV curves for the supercapacitor device at various numbers of cycles. The inset figure shows the % retention of the specific capacitance as a function of the number of cycles.

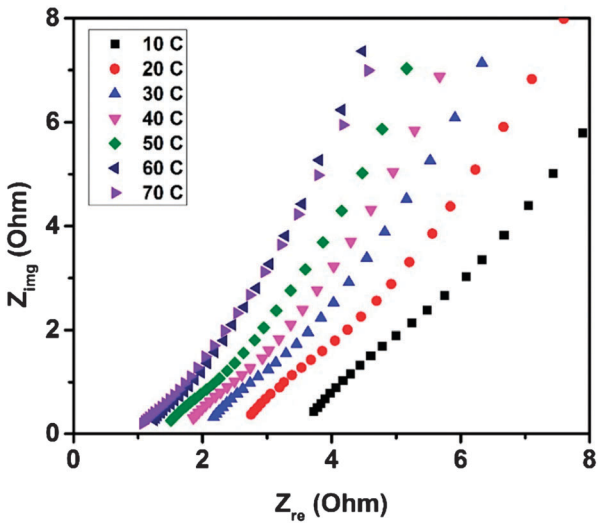

Fig. 13 Z_{re} *vs.* Z_{img} plots (Nyquist plots) for the device at various temperatures.

The increase in the capacitance of the device with increasing temperature was analyzed using electrochemical impedance spectroscopy (EIS). The main objective of the EIS measurements was to gain insight into the temperature dependence of the resistive and capacitive elements, and their effects on the performance of the supercapacitor device. Fig. 13 shows the EIS spectra of the device at various temperatures. As seen in the figure, the equivalent series resistance (ESR) for the device decreases with increasing temperature. The decrease in the ESR value could be due to the enhanced mobility of the ions in the electrolyte, which increases the conductivity of the electrolyte.[44] Therefore, the reduced ESR at higher temperature plays a key role in improving the charge storage capacity of the device. The impedance of the device was also observed to decrease with increasing temperature and frequency (Fig. S7, ESI†). Meng *et al.*[45] also observed an improvement in the capacitance with temperature for a porous Fe_3O_4–carbon composite electrode. The present study indicates that cobalt molybdate could be a promising material for flexible charge storage device with the additional advantage of improved charge storage at high temperature.

4. Conclusions

Cobalt molybdates with varying morphology were synthesized using a hydrothermal method. The present study provides a new feature to change the growth conditions to yield different morphologies such as cauliflowers, bricks and nano-spheres. The charge storage capacity of these materials was examined using electrochemical techniques. The cyclic voltammograms of the cobalt molybdate electrodes showed typical pseudocapacitive behavior. The charge storage capacity was observed to depend on the morphology of cobalt molybdate. The highest specific capacitance of 259 F g^{-1} at the current of 1 mA in a 3 M NaOH was observed with great cyclic stability for nano-sphered cobalt molybdate. These electrodes showed great flexibility with no degradation in the charge-storage capacity. In addition to flexibility, high charge storage capacity and cyclic stability, they offer robust performance at evaluated temperature. The specific capacitance of the cobalt molybdate device showed about 386% improvement in the charge storage capacity when the working temperature was elevated from 10 to 70 °C. Hence, this study provides a new facile method to synthesize morphology controlled cobalt molybdates for the next generation of flexible energy storage devices for high-temperature applications.

Acknowledgements

The authors wish to thank Pittsburg State University for providing financial support. This material is based upon the work supported by the National Science Foundation under Award No. EPS-0903806 and matching support from the State of Kansas through the Kansas Board of Regents.

References

1 R. Kötz and M. Carlen, *Electrochim. Acta*, 2000, **45**, 2483–2498.
2 Y. Zhang, H. Feng, X. Wu, L. Wang, A. Zhang, T. Xia, H. Dong, X. Li and L. Zhang, *Int. J. Hydrogen Energy*, 2009, **34**, 4889–4899.
3 A. Burke, *Electrochim. Acta*, 2007, **53**, 1083–1091.
4 H. R. Ghenaatian, M. F. Mousavi and M. S. Rahmanifar, *Synth. Met.*, 2011, **161**, 2017–2023.
5 B. E. Conway, V. Birss and J. Wojtowicz, *J. Power Sources*, 1997, **66**, 1–14.
6 J.-L. Shi, W.-C. Du, Y.-X. Yin, Y.-G. Guo and L.-J. Wan, *J. Mater. Chem. A*, 2014, **2**, 10830–10834.
7 A. Burke, *J. Power Sources*, 2000, **91**, 37–50.
8 C. Ashtiani, R. Wright and G. Hunt, *J. Power Sources*, 2006, **154**, 561–566.
9 A. Chu and P. Braatz, *J. Power Sources*, 2002, **112**, 236–246.
10 A. Burke and M. Miller, *J. Power Sources*, 2011, **196**, 514–522.
11 T. Chen and L. Dai, *J. Mater. Chem. A*, 2014, **2**, 10756–10775.
12 E. Mitchell, R. K. Gupta, K. Mensah-Darkwa, D. Kumar, K. Ramasamy, B. K. Gupta and P. Kahol, *New J. Chem.*, 2014, **38**, 4344–4350.
13 E. Mitchell, F. De Souza, R. K. Gupta, P. K. Kahol, D. Kumar, L. Dong and B. K. Gupta, *Powder Technol.*, 2015, **272**, 295–299.
14 H. Wang, Y. Wang and X. Wang, *New J. Chem.*, 2013, **37**, 869–872.
15 J. Chen, K. Huang and S. Liu, *Electrochim. Acta*, 2009, **55**, 1–5.
16 L. Yang, S. Wang, J. Mao, J. Deng, Q. Gao, Y. Tang and O. G. Schmidt, *Adv. Mater.*, 2013, **25**, 1180–1184.
17 Y. Gao, S. Chen, D. Cao, G. Wang and J. Yin, *J. Power Sources*, 2010, **195**, 1757–1760.
18 L. Qian, L. Gu, L. Yang, H. Yuan and D. Xiao, *Nanoscale*, 2013, **5**, 7388–7396.
19 U. M. Patil, S. B. Kulkarni, V. S. Jamadade and C. D. Lokhande, *J. Alloys Compd.*, 2011, **509**, 1677–1682.
20 P. M. Kulal, D. P. Dubal, C. D. Lokhande and V. J. Fulari, *J. Alloys Compd.*, 2011, **509**, 2567–2571.
21 J.-G. Wang, Y. Yang, Z.-H. Huang and F. Kang, *J. Power Sources*, 2012, **204**, 236–243.
22 W.-H. Jin, G.-T. Cao and J.-Y. Sun, *J. Power Sources*, 2008, **175**, 686–691.
23 X. Yan, X. Tong, J. Wang, C. Gong, M. Zhang and L. Liang, *J. Alloys Compd.*, 2014, **593**, 184–189.
24 Y. Hou, L. Chen, P. Liu, J. Kang, T. Fujita and M. Chen, *J. Mater. Chem. A*, 2014, **2**, 10910–10916.
25 Y. Qian, R. Liu, Q. Wang, J. Xu, D. Chen and G. Shen, *J. Mater. Chem. A*, 2014, **2**, 10917–10922.
26 Y. Liu, J. Zhang, S. Wang, K. Wang, Z. Chen and Q. Xu, *New J. Chem.*, 2014, **38**, 4045–4048.
27 J. Feng, X. Sun, C. Wu, L. Peng, C. Lin, S. Hu, J. Yang and Y. Xie, *J. Am. Chem. Soc.*, 2011, **133**, 17832–17838.
28 K. Krishnamoorthy, G. K. Veerasubramani, S. Radhakrishnan and S. J. Kim, *Chem. Eng. J.*, 2014, **251**, 116–122.
29 D. Cai, B. Liu, D. Wang, Y. Liu, L. Wang, H. Li, Y. Wang, C. Wang, Q. Li and T. Wang, *Electrochim. Acta*, 2014, **115**, 358–363.

30 L.-Q. Mai, F. Yang, Y.-L. Zhao, X. Xu, L. Xu and Y.-Z. Luo, *Nat. Commun.*, 2011, **2**, 381.
31 D. Cai, D. Wang, B. Liu, Y. Wang, Y. Liu, L. Wang, H. Li, H. Huang, Q. Li and T. Wang, *ACS Appl. Mater. Interfaces*, 2013, **5**, 12905–12910.
32 X. Xia, W. Lei, Q. Hao, W. Wang and X. Wang, *Electrochim. Acta*, 2013, **99**, 253–261.
33 G. K. Veerasubramani, K. Krishnamoorthy, S. Radhakrishnan, N.-J. Kim and S. J. Kim, *Int. J. Hydrogen Energy*, 2014, **39**, 5186–5193.
34 X. Xu, J. Shen, N. Li and M. Ye, *J. Alloys Compd.*, 2014, **616**, 58–65.
35 M.-C. Liu, L.-B. Kong, X.-J. Ma, C. Lu, X.-M. Li, Y.-C. Luo and L. Kang, *New J. Chem.*, 2012, **36**, 1713–1716.
36 F. Zhao, Y. Wang, X. Xu, Y. Liu, R. Song, G. Lu and Y. Li, *ACS Appl. Mater. Interfaces*, 2014, **6**, 11007–11012.
37 L.-J. Xie, J.-F. Wu, C.-M. Chen, C.-M. Zhang, L. Wan, J.-L. Wang, Q.-Q. Kong, C.-X. Lv, K.-X. Li and G.-H. Sun, *J. Power Sources*, 2013, **242**, 148–156.
38 C. Xiang, M. Li, M. Zhi, A. Manivannan and N. Wu, *J. Power Sources*, 2013, **226**, 65–70.
39 W. Tang, S. Tian, L. L. Liu, L. Li, H. P. Zhang, Y. B. Yue, Y. Bai, Y. P. Wu and K. Zhu, *Electrochem. Commun.*, 2011, **13**, 205–208.
40 J. Gomez and E. E. Kalu, *J. Power Sources*, 2013, **230**, 218–224.
41 S. H. Mujawar, S. B. Ambade, T. Battumur, R. B. Ambade and S.-H. Lee, *Electrochim. Acta*, 2011, **56**, 4462–4466.
42 Y. F. Yuan, X. H. Xia, J. B. Wu, X. H. Huang, Y. B. Pei, J. L. Yang and S. Y. Guo, *Electrochem. Commun.*, 2011, **13**, 1123–1126.
43 O. Ghodbane, J.-L. Pascal and F. Favier, *ACS Appl. Mater. Interfaces*, 2009, **1**, 1130–1139.
44 W. Li, K. Xu, L. An, F. Jiang, X. Zhou, J. Yang, Z. Chen, R. Zou and J. Hu, *J. Mater. Chem. A*, 2014, **2**, 1443–1447.
45 W. Meng, W. Chen, L. Zhao, Y. Huang, M. Zhu, Y. Huang, Y. Fu, F. Geng, J. Yu, X. Chen and C. Zhi, *Nano Energy*, 2014, **8**, 133–140.

